Geophys. J. R. astr. Soc. (1987) **91**, 501–516

Measuring anisotropy in rocks using laser-generated ultrasound

R. Paul Young and David A. Hutchins *Departments of Geological Sciences and Physics, Queen's University, Kingston K7L 3N6, Canada*

Accepted 1987 July 27. Received 1987 July 27; in original form 1987 May

Summary. Measurements using standard contacting piezoelectric transducers and non-contacting laser sources and detectors, have been investigated for the study of ultrasonic anisotropy in rocks. An ultrasonic polariscope has been constructed in order to obtain reproducible travel-time and amplitude measurements. Three case studies are described to demonstrate the apparatus, namely isotropic halite, anisotropic calcite and transversely anisotropic mudstone. A novel technique has been developed in order to construct pseudo-particle motion diagrams, to highlight shear-wave birefringence in rock samples using 2.25 MHz transducers. A pulsed laser has been used to generate compressional and shear waves for comparison with piezoelectric transducer results. The pulses generated by laser irradiation have many advantages for the study of velocity and attenuation anisotropy because of their known characteristics, broad bandwidth and high level of reproducibility. The use of a non-contacting laser source and detector eliminates the need for elaborate coupling agents, stress bonding or immersion techniques. Point-source and line-focusing of the laser beam provides an indirect method of studying shear-wave polarization phenomena. Results from rotation of the line-focused laser beam and rotation of piezoelectric shear-wave transducers with respect to anisotropy, are compared for both velocity and amplitude phenomena in an anisotropic rock sample.

1 Introduction

Anisotropy in rocks is a result of many factors including variation in material properties, as well as crack and stress effects. In general, shear waves travelling in an anisotropic medium split into two components with different velocities and polarizations. This phenomenon is known as shear-wave birefringence and is analogous to the double refraction effect observed when thin rock sections are viewed under a petrological polarizing microscope. The character-

istics of wave propagation in anisotropic rocks are governed by the anisotropic symmetry. The situation outlined above is typical for transversely anisotropic rock or hexagonal symmetry where five elastic constants uniquely define the material. However, as the symmetry reduces, as many as 21 elastic constants are required to define the properties of the rock. This is compared with the isotropic case where two elastic constants (two seismic wave velocities – one compressional and one shear) are sufficient to define the elastic properties of the material. This additional complexity can result in very intricate wave propagation with multiple wave-arrivals for lower symmetry classes of anisotropy. The derivation of the characteristic equation and its solution for the various symmetry classes of anisotropy is given by Musgrave (1954a, b, 1970) and Vlaar (1968).

Although shear-wave anisotropy was observed from earthquake records as early as 1938 (Byerly 1938) and from small-scale refraction survey results in 1956 (Jolly 1956), it has been the relatively recent resurgence of interest in the phenomenon which has resulted in more detailed field and theoretical studies (Bamford & Crampin 1977; Crampin, Chesnokov & Hipkin 1984; Crampin 1985). The pioneer laboratory experimental work on shear-wave birefringence in rocks is generally attributed to Nur & Simmons (1969a, b), although the effect was observed in crystals much earlier by Aleksandrov (1956a, b). Prior to this, laboratory experimental work concentrated on the use of compressional waves to study rock anisotropy. These experiments involved the measurement of travel times in different directions in the specimen and, consequently, variations due to different travel paths needed to be considered. One of the advantages of using shear waves to study anisotropy is that the same travel path can be used. In addition, compressional velocities vary significantly as a function of saturation, but this has a minimal effect on shear waves. Notable material shear-wave anisotropic studies have been carried out in slate and dunite by Christenson (1971) and Christensen & Ramananantoandro (1971), and other rock types by Tilmann & Bennett (1973), while stress and crack anisotropy has been studied by Nur & Simmons (1969a, b) and Bonner (1974).

The coupling of the transducers and/or the reproducibility of the source are major factors in any detailed study of amplitude phenomena. This paper shows how modified optic bench components have been used to construct an ultrasonic polariscope. This system has been used with traditional piezoelectric (PZT) transducers to minimize the coupling problem. The results from these PZT experiments are compared with results obtained by using a pulsed laser as an ultrasonic source. An overview of the theory for laser irradiation in solids is given, together with a case study for anisotropic rock. Results from two mineral crystals (isotropic halite and anisotropic calcite) and one rock sample (anisotropic mudstone) are discussed. The theory of wave propagation in anisotropic media is discussed in detail by other authors, notably Vlaar (1968) and Hudson (1981), and is therefore not described here. This paper concentrates on experimental results of shear-wave birefringence and amplitude phenomena obtained when selected anisotropic minerals and rocks are investigated using laser irradiation and PZT transducers.

2 Laser generation of ultrasonic waves

Laser generation of ultrasonic waves in rocks does not seem to have been reported in the literature, although the method is now well established for use in a range of media including solids, liquids and gases (Hutchins 1986) and porous media (Hutchins, Young & Ungar 1985). A brief overview of the advantages and characteristics of the laser-generated ultrasonic source is now given.

The laser source does not require any physical contact with the specimen and inaccuracies

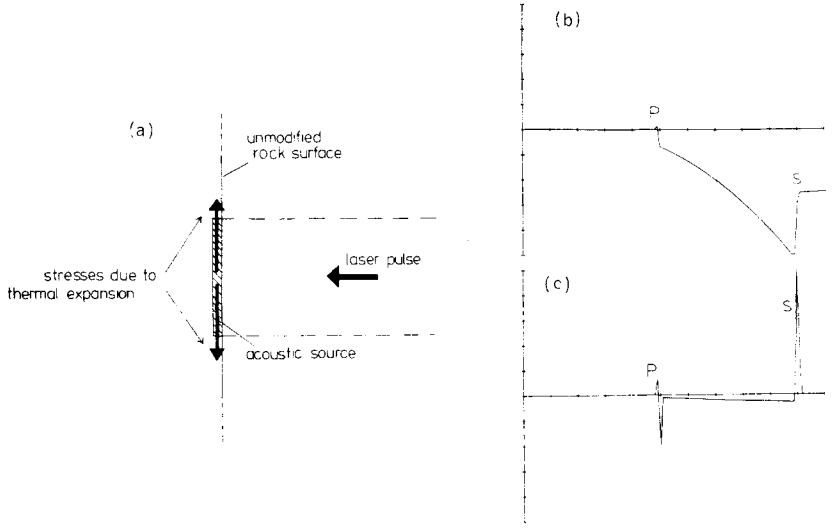

Figure 1. (a) Schematic of thermoelastic ultrasonic source mechanism induced by pulsed laser irradiation. (b) Resultant displacement waveform at the opposite surface of a solid specimen (Poisson's ratio = 0.3). (c) Corresponding velocity waveform.

due to coupling between the sample and transducer are minimized. Further, the laser pulse itself can be used to trigger a time base and extremely accurate triggering is possible. In addition, the use of a short laser pulse (30 ns in this work) leads to a very broad spectral content, useful in ultrasonic spectroscopy.

Two principal mechanisms may be used for ultrasonic generation at a solid surface. The first involves thermal expansion of the solid following the absorption of optical energy from the incident laser pulse. The amount of energy absorbed by the surface is the integral of the laser pulse shape and is step-like in time. This mechanism results in thermal expansion close to the solid surface, at a depth limited by thermal diffusion. Thermal stresses parallel to the solid surface tend to dominate as those perpendicular to it are not present due to boundary

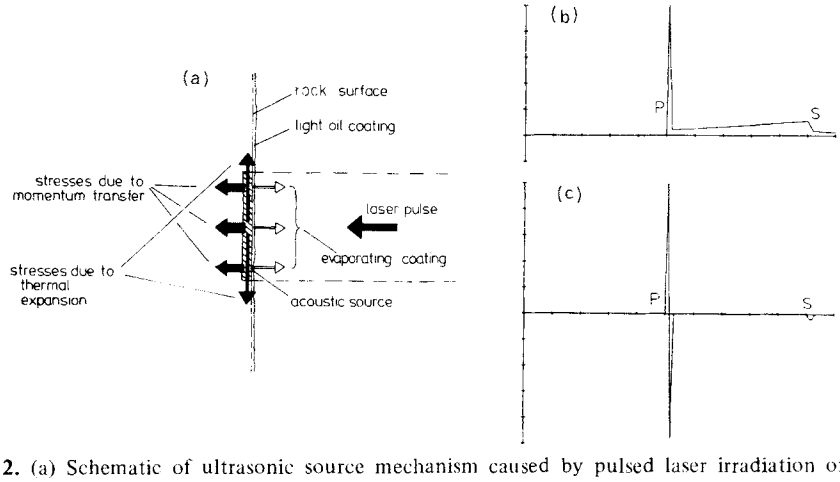

Figure 2. (a) Schematic of ultrasonic source mechanism caused by pulsed laser irradiation of a liquid coated surface. (b)Resultant displacement waveform at the opposite surface of a solid specimen (Poisson's ratio = 0.3). (c) Corresponding velocity waveform.

conditions. This type of source mechanism is shown schematically in Fig. 1(a) and it can be seen that the laser generates a radial expansion of thermal stresses equivalent to a set of force dipoles parallel to the surface. Wave propagation theory (Pao & Gajewski 1977) may be used to predict the ultrasonic waveform radiated by such a source and the results are presented in Fig. 1(b) and (c) for normal displacement and velocity, respectively (Hutchins & Wilkins 1985a). It should be noted that the shear-wave motion is larger than that of the compressional mode, as might be expected from such a source. In fact, for a material with a Poisson's ratio of 0.3, the predicted shear-wave amplitude is approximately four times that of the compressional mode.

The second principal mechanism of generating ultrasound using a laser source involves the evaporation of a coating applied to one surface of the solid. The incident laser-pulse evaporates the coating material and a recoil mechanism causes a force normal to the surface to be established. This source mechanism is shown schematically in Fig. 2(a) superimposed on stresses that may be present due to thermal effects. If the thermal effects are negligible, wave propagation theory can be used to predict the displacement and velocity waveforms resulting from such a mechanism (see Fig. 2b and c). It should be noted that for this mechanism of laser-generated ultrasound, the compressional wave dominates the signal and is monopolar in displacement and hence bipolar in velocity. The waveforms given in Figs 1 and 2 are for aligned source and receiver positions, as the signal characteristics change significantly when the receiver is moved off-axis away from this position. Directivity patterns of such source effects have been discussed elsewhere (Hutchins 1986), but in this study, the thermal expansion mechanism has been used with aligned source and receiver positions in order to efficiently generate enhanced shear modes.

An additional advantage of the pulsed laser technique is that the shape of the source may be changed by the use of lenses and apertures. The use of a cylindrical lens, for example, results in a line focus from which a degree of polarization of shear waves can be achieved following thermal expansion (Hutchins & Wilkins 1985b). This line-focused laser source and the circular polarization thermal-expansion source are used in this study to generate ultrasonic pulses in a rock sample for the determination of shear-wave birefringence.

3 Instrumentation and experiments

Two groups of experiments were carried out for the investigation of laboratory shear-wave birefringence. The first used standard PZT transducers for both source and receiver, while the second used a pulsed laser to generate the ultrasonic wave. The instrumentation for both types of experiments are described separately below.

3.1 PZT TRANSDUCER EXPERIMENTS USING AN ULTRASONIC POLARISCOPE

In order to obtain reproducible waveform measurements from PZT transducers for the study of shear-wave birefringence phenomena an ultrasonic polariscope was constructed. This was achieved by utilizing commercially available optic bench equipment (Ealing Optics) and modifying it to accommodate mineral/rock samples and PZT transducers, rather than optical lenses. This system allowed the specimen to be positioned to an accuracy of 0.1 mm and rotated with an accuracy of 0.5°. Two precision stages (similar to a microscope rotating stage) were modified and used to hold PZT transducers on either side of the specimen holder. The transducer holder was spring mounted and the spring constant could be varied. The transducer holders could also be moved in space with precision movement devices to the same accuracy as the specimen holder. The two transducer holders and specimen holder were

then fixed to an optic bench, which used a rack and pinion system to provide precision linear movement along the bench. The specimens were polished and coated with a thin film of honey to provide good acoustical coupling between transducer and sample. The amount of pressure which each transducer placed on the specimen could be reproduced by using the optic bench to precisely position the specimen and transducers. The spring-mounted transducers would exert a pressure equal to the displacement of the spring multiplied by the spring constant. After the polariscope had been set up, the reproducibility could be tested for different orientations of the transducer axis by rotating the transducers on their honey film through 360°. This test produced reproducible waveforms for measurements taken through the whole 360° rotation of the transducers. Measurements using this apparatus were usually taken after the transducers had been rotated through two revolutions on the honey film and the whole procedure repeated after the honey film had gone through more than five revolutions. This set procedure allowed measurements to be taken using both compressional and shear-wave transducers on the same sample and in the same position, for subsequent construction of pseudo-particle motion diagrams.

Particle motion diagrams (hodographs) have been found by the authors to be extremely useful in identifying the arrival of various wave phases on tri-axial seismogram records. However, it is not possible to build a scaled version of a triaxial seismometer for ultrasonic work in the MHz range. In the field, the wavelength of the seismic wave is always signifi-

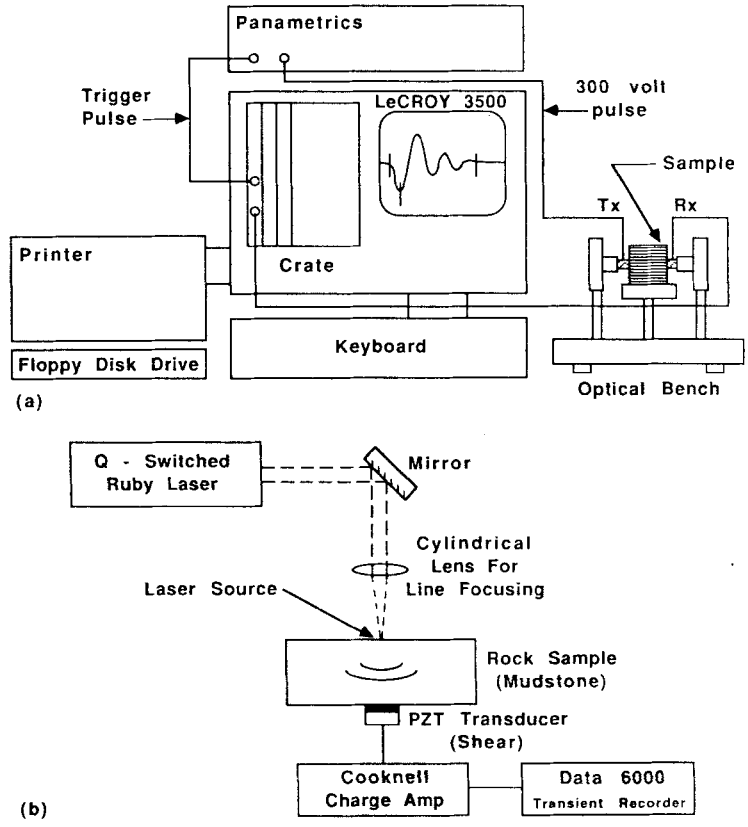

Figure 3. (a) Schematic of ultrasonic instrumentation using PZT transducers and modified optic bench polariscope. (b) Instrumentation schematic for pulsed-laser generation of ultrasonic waves.

cantly larger than the size of the transducer. In the laboratory, however, the wavelengths at MHz frequencies are in the mm range and therefore it is almost impossible to build a MHz triaxial sensor. This is the primary reason why particle motion diagrams have not been constructed for laboratory experiments. One solution to this problem is to produce a system which is capable of reproducible amplitude measurement and then collect the three axes of information sequentially rather than concurrently. This approach allows the three axes to be combined and traditional particle motion diagrams to be plotted. The apparatus outlined above has been used to obtain such waveforms and thereby facilitate the construction of pseudo-particle motion diagrams for the investigation of shear-wave birefringence.

The instrumentation system used is shown schematically in Fig. 3(a). The polariscope transmitter transducer (Tx) was pulsed with a high-voltage spike transient from a Panametrics ultrasonic analyser. The waveforms from the polariscope receiver transducer (Rx) were amplified and digitized using a Lecroy 3500 waveform analyser sampling at 32 MHz. The analogue to digital conversion gave a dynamic range and resolution of eight bits (48 dB). Enhanced dynamic range was achieved by signal averaging which was carried out by adding 1000 waveforms into the transient recorder memory. Thus the amplitude range on Figs 4–7 is 0–255 000 with absolute values depending on system gain. The transducers used were Panametrics 12.5 mm diameter, 2.25 MHz units, with individual shear and compressional units being used for the experiments. These transducers were chosen because they represented an almost perfectly damped velocity transducer. The waveforms for these transducers were compared with an interferometer detector using a laser ultrasonic source and the output obtained was very similar to the predicted velocity waveform.

Three samples were studied using this apparatus, isotropic halite, anisotropic calcite and a strongly anisotropic mudstone from the coal measures sequence of Northern England. A halite crystal was chosen because it is optically isotropic, in contrast to calcite which is known to have an extremely large optical birefringence. The calcite experiment was made more complex in that the crystal faces for calcite are not parallel to the optic axis. The mudstone sample was chosen because it was known to have a good seismic anisotropy.

3.2 LASER ULTRASOUND SYSTEM

Fig. 3(b) shows schematically the experimental apparatus for the generation and detection of laser-induced ultrasound. A *Q*-switched ruby laser of approximately 1 J and pulse duration of 30 ns, was directed upon one face of the rock specimen. Dielectric mirrors were used to direct the beam on to the surface. A helium/neon continuous laser, with its axis coincident with the ruby laser optics, was used to position the sample correctly. The laser beam was focused using silica lenses to produce either symmetric or line foci at the sample.

Ultrasonic waves travelled through the sample and were detected at its far surface using a 1 MHz Panametrics shear-wave PZT transducer mounted in one of the holders of the polariscope shown in Fig. 3(a), the other transducer holder being removed for this measurement to allow easy access for the laser beam. In common with the PZT measurement system above, the shear-wave transducer was rotated about its axis to sample various directions of shear-wave polarization within the sample. Signals from the Rx were amplified and recorded digitally using a Data Precision Data 6000 transient recorder, with an eight-bit resolution and a maximum sampling rate of 100 MHz.

Experiments were conducted using the thermal expansion mechanism for both a circular source of 12.5 mm diameter (equal to that of the PZT receiver) and a 15 x 1.5 mm line source produced with the aid of a cylindrical lens. The cylindrical lens could be rotated about its axis, so that the orientation of the line source and hence any polarization could be varied

with respect to the sample anisotropy and shear-wave detector alignment. In addition, it was possible to focus the laser beam more sharply with a layer of vacuum grease or machine oil applied to the generating surface. This resulted in the evaporation/momentum transfer source shown schematically in Fig. 2 and more efficient compressional wave generation.

4 Results and discussion

Results are presented for the three experiments using the ultrasonic polariscope and PZT transducers in halite, calcite and mudstone. The main function of the halite and calcite experiments was to investigate the effectiveness of the modified optic bench apparatus for the measurement of ultrasonic parameters, using materials of known physical properties. Pseudo particle-motion diagrams are generated to highlight the shear-wave birefringence, and amplitude data for both fast and slow shear waves as a function of the polarization and specimen anisotropy, are also outlined. The laser experimental results are then given for both point and line sources in mudstone. Laser irradiation was not carried out on the mineral samples because they were transparent and therefore laser light was able to enter the sample, making ultrasonic wave generation more complicated. Tests are currently underway to study transparent minerals after they have been coated with materials which inhibit the propagation of laser light into the sample. This is clearly not a problem with the majority of rock samples. The results described for the three samples highlight the major ultrasonic birefringence effects, although theoretically, additional polarization phenomena may be present for measurements taken in different directions and for non-aligned source and receiver positions.

4.1 PZT ULTRASONIC POLARISCOPE MEASUREMENTS

4.1.1 Isotropic halite

Halite is a mineral with cubic symmetry and it is optically isotropic. Light travelling through halite does not exhibit double refraction and shows no optical birefringence (difference in refractive indices). By analogy, ultrasonic shear waves might therefore be expected to maintain a single polarization while propagating through halite. A crystal of halite was tested in the polariscope and Fig. 4 gives example waveforms obtained from rotating the PZT shear wave transducers while keeping the orientation of the crystal fixed. The waveform in Fig. 4(a) is the calibration wave with no specimen between Tx and Rx. The waveforms in Fig. 4(b) and (c) show the arrival time of the pulse, delayed due to passing through the sample of halite. The transducers were placed on the 100 and $\bar{1}00$ (Miller indices) crystal faces. The orientation of shear-wave polarization is shown for 045° and 080° rotation on the crystal face. It can be seen clearly that the waveform shape and arrival time do not change with rotation. Measurements were made every 15° and minimal change in shear-wave velocity or wave shape was observed. The measured compressional velocity was 4650 $m\,s^{-1}$, with a uniform shear wave velocity for all angles of rotation of 2385 ms^{-1}. Fig. 4(d) shows the amplitude of the Rx rotated through 180° for two Tx orientations. The measured amplitude is the major peak on the waveform and is identifiable on each of the waveforms for all rotation angles. The amplitudes increase to a maximum when the Tx and Rx are parallel and go to almost zero when the Rx and Tx are perpendicular. It is clear that the Rx is measuring a component of the input waveform. If the measured peak amplitude is multiplied by the cosine of the angle between the Tx and Rx, an expected amplitude for the given orientation can be obtained. For the results shown in Fig. 4(d), the actual and expected

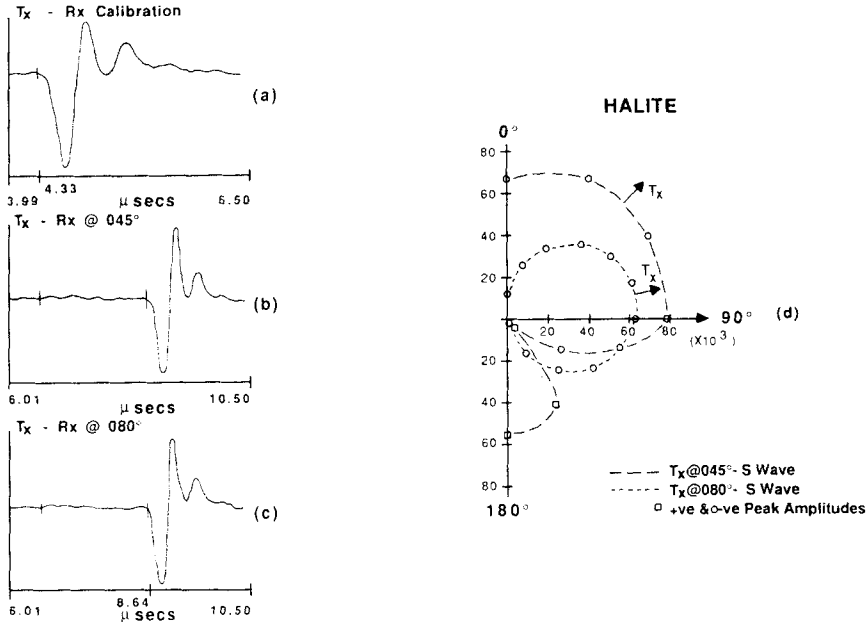

Figure 4. Travel-time and amplitude measurements in isotropic halite. (a) Tx–Rx calibration waveform. (b) Waveform when Tx–Rx polarizations orientated parallel to each other at 045°. (c) Waveform when Tx–Rx polarizations orientated parallel to each other at 080°. (d) Relative Rx amplitude measurements for two Tx orientations (indicated by arrows).

amplitudes are extremely similar. The differences observed reflect minor reproducibility problems in the apparatus. Fig. 4(d) shows that the peak amplitudes depend on the Tx orientation and not any property within the halite. The halite sample does not exhibit any ultrasonic birefringence (anisotropic velocity difference). The differences in amplitude between Tx(045°) and Tx(080°) measurements indicate that reproducibility is not as good between tests as within tests. This is a function of removing the transducers from the specimen and re-establishing the coupling after several rotations of the Rx. Within a single rotation experiment, the measurements were quite reproducible, giving similar results for up to three rotations of the Rx.

4.1.2 Anisotropic calcite

Calcite is a trigonal, optically uniaxial mineral which displays rhombohedral cleavage. This results in the *c*-crystallographic-axis and the coincident optic-axis being at an angle to the crystal faces. It might therefore be expected that ultrasonic birefringence would occur in directions non-normal to the optic axis. The Tx and Rx were positioned on the $10\bar{1}1$ and $\bar{1}01\bar{1}$ crystal faces. If the *c*-axis is projected on to the $10\bar{1}1$ crystal face, it makes an angle of approximately 50°. Calcite has a very high optical birefringence of 0.172 with the *c*-axis being the ordinary optical axis. Thus the velocity of light is fastest parallel to the *c*-axis and by analogy, the fast shear-wave might be expected to be polarized in the direction of the *c*-axis, with the slow wave being polarized at 090° to this direction. Fig. 5 shows three example waveforms from parallel Tx and Rx rotation on the calcite crystal. The waveform in Fig. 5(a) shows the arrival of the fast shear-wave, when the transducer is polarized within 005° of parallel to the *c*-axis projection on to the crystal face. The waveform in Fig. 5(b) is

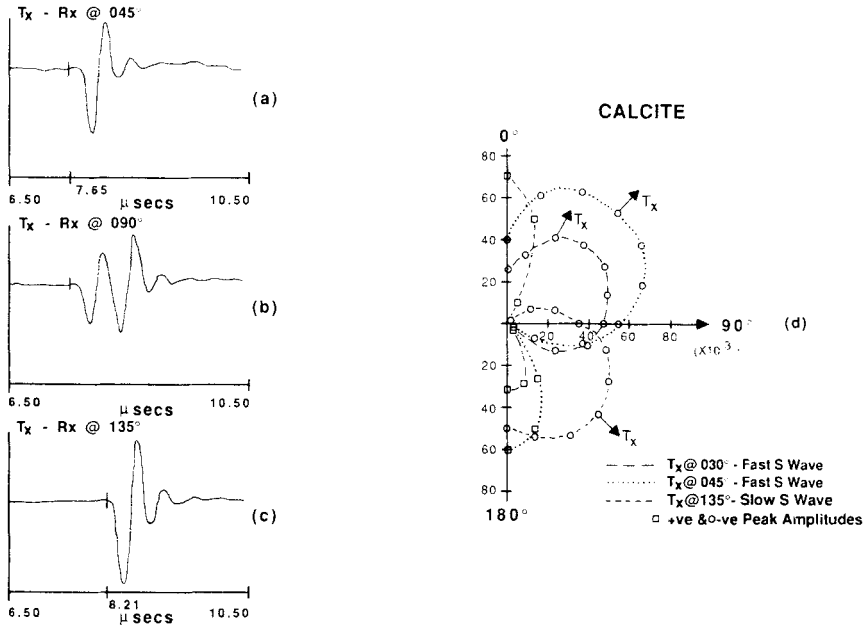

Figure 5. Travel-time and amplitude measurements in anisotropic calcite. (a) Waveform of fast shear wave when Tx–Rx polarizations orientated parallel to each other and parallel to optic axis. (b) Waveform when Tx–Rx polarizations orientated at 045° to optic axis direction; both the fast and slow shear-waves are present. (c) Waveform of slow shear wave when Tx–Rx polarizations orientated perpendicular to the optic axis. (d) Relative Rx amplitude measurements of fast and slow shear waves for three Tx orientations (indicated by arrows).

obtained when the Tx and Rx are polarized 045° to the *c*-axis and is the combination of both fast and slow waves. The waveform in Fig. 5(c) shows the arrival of the slow wave when the Tx and Rx are polarized almost perpendicular to the *c*-axis. It should be noted that the shape of the waveform for both the slow and fast wave is very similar to the calibration waveform shown in Fig. 4(a).

It can be seen that the calcite is displaying strong ultrasonic birefringence. The compressional wave velocity is 7210 ms^{-1}, with a fast shear-wave velocity of 3100 ms^{-1} and a slow shear-wave velocity of 2650 ms^{-1}. Thus the resulting ultrasonic birefringence of the calcite is 450 ms^{-1}. Fig. 5(d) shows the amplitude of the Rx rotated through 180° for three Tx orientations. The diagram shows how the amplitudes increase to a maximum at the Rx position which is parallel to the polarization direction of the wave being measured. With the Tx polarization at 045°, the fast wave amplitude is maximum at 045° and with the Tx at 030°, the fast wave amplitude is also maximum at approximately 045°. When the Tx polarization is at 135°, it can be seen that the slow wave is a maximum at 135°. The amplitude data confirm the position of the fast polarization axis close to 045°, with the slow polarization direction close to 135°. This is in good agreement with the known optic axis fast orientation being at approximately 050° and slow direction at 140°. The slight error is caused by the measurements being taken at 015° increments, but additional data points around the polarization axes resolve this error.

4.1.3 Anisotropic mudstone

The mudstone sample is composed of 5 per cent quartz, 2 per cent feldspar, 1 per cent muscovite, 1 per cent carbonaceous material and >90 per cent matrix material. The matrix

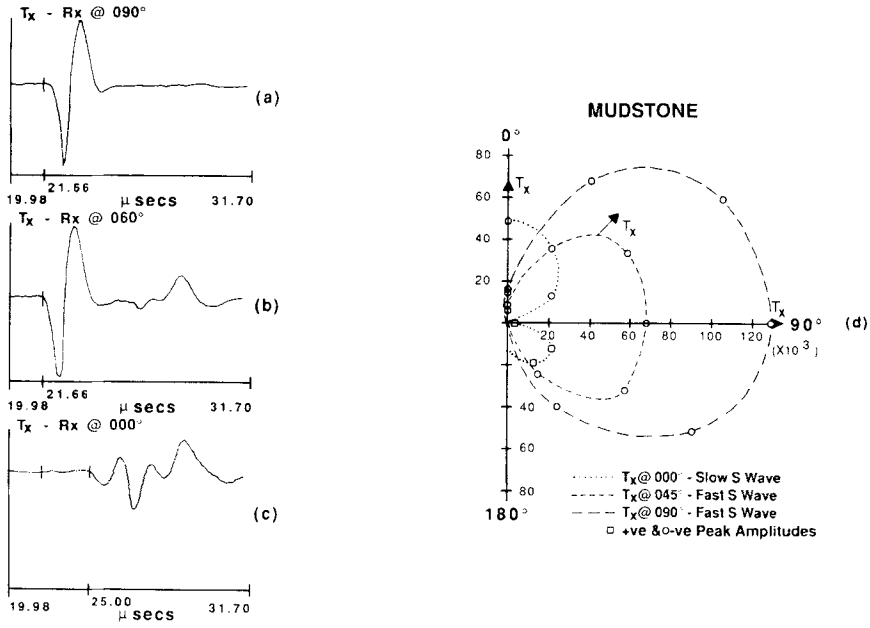

Figure 6. Travel-time and amplitude measurements in transversely anisotropic mudstone. (a) Waveform of fast shear wave when Tx–Rx polarizations orientated parallel to each other and parallel to microlaminations. (b) Waveform when Tx–Rx polarizations orientated at an angle to the micro-lamination; both the fast and slow shear waves are present. (c) Waveform of predominantly slow shear wave when Tx–Rx polarizations orientated perpendicular to the microlamination. (d) Relative amplitude measurements of fast and slow shear waves for three Tx orientations (indicated by arrows).

is composed of very fine-grained illite and kaolinite which form an orientated platy texture, resulting in measurable seismic anisotropy. The specimen was considered to be transversely anisotropic and was chosen because the grain size was considerably less than the wavelength. The rock faces were polished and the Tx and Rx transducers were placed on the faces displaying the microlamination. This resulted in the microlamination being parallel with the Tx and Rx assembly when it was rotated to the 090° position. Fig. 6 shows three example waveforms of parallel Tx and Rx rotation on the rock sample. The waveform in Fig. 6(a) displays the fast shear wave observed at the 090° position. Note the similarity to the calibration waveform given for halite in Fig. 4(a). The waveform in Fig. 6(b) is for a rotation of 060° and shows the dominance of the fast wave, but the slow shear-wave is starting to develop. The waveform in Fig. 4(c) is for 000° position and shows a more complex waveform than those shown for calcite in a similar orientation. The slow wave is clearly visible but the fast wave has not decayed to zero. In addition, a further arrival of large amplitude can be seen, which is thought to be associated with normal mode propagation and channelling effects caused by the microlamination anisotropy.

It can be seen that the mudstone is displaying ultrasonic birefringence. The compressional wave velocity is $3770\,ms^{-1}$, with a fast shear-wave velocity of $2460\,ms^{-1}$ and a slow shear-wave velocity of $2190\,ms^{-1}$. Thus the resulting ultrasonic birefringence in the mudstone is $270\,ms^{-1}$. Fig. 6(d) shows the amplitude of the Rx rotated through 180° for three Tx orientations. The diagram shows how the amplitudes increase to a maximum at the Rx position, which is parallel to the polarization direction of the wave being measured. With the Tx in the 045° and 090° position, the maximum Rx fast wave amplitude is in the 090°

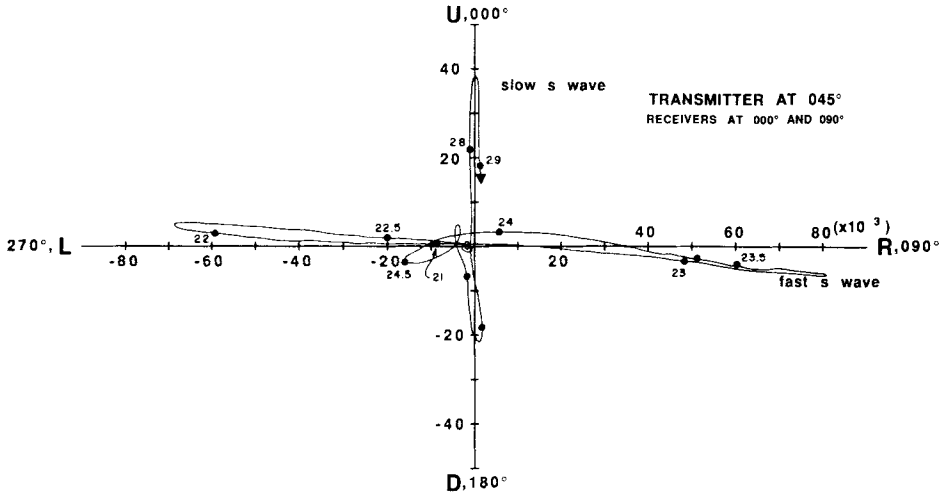

Figure 7. Pseudo-particle motion diagram for a 2.25 MHz ultrasonic waveform in anisotropic mudstone obtained for a Tx orientation at 045° to the microlamination and Rx orientations parallel and perpendicular to the microlamination; particle motion shown from 20–29 μs to highlight the fast and slow shear waves.

position. With the Tx in the 000° position, the maximum slow wave amplitude is in the 000° position. This pattern is very similar to that displayed for the calcite crystal. However, in this case the fast direction is 090° which is parallel to the microlamination in the sample. The deviations from a perfect pattern on Fig. 6(b) are thought to be a result of the specimen not being uniformly transversely anisotropic.

Fig. 7 shows a pseudo particle-motion diagram for the mudstone sample. This Tx was oriented at 045° and separate measurements were taken with the shear-wave Rx at 000° and 090°. These measurements were taken over the same time window, thus facilitating the amplitudes to be cross-plotted to obtain a pseudo particle-motion diagram. The diagram shows the particle motion of arriving waves in the window 21–29 μs. This window covers the arrival of both the fast and slow shear waves. It can be seen that the fast wave, vibrating 090°–270°, arrives ahead of the slow wave, vibrating 000°–180°. It is also possible to see that the fast-wave amplitude is approximately double the slow-wave amplitude.

4.2 LASER MEASUREMENTS IN ANISOTROPIC MUDSTONE

The pulsed laser source was used, as shown in Fig. 3(b), to investigate ultrasonic birefringence in the same mudstone sample as that described in the preceding section. In the first series of experiments, a circular-shaped source was formed by placing an aperture of 12.5 mm diameter between the ruby laser and the specimen. The optical power-density at the mudstone surface was sufficiently low that the surface was not damaged; hence ultrasonic generation occurred via the thermal expansion mechanism.

Fig 1(c) is the predicted velocity waveform at a solid suface assuming an isotropic medium and shows the dominance of a single shear mode. Fig. 8(a) is the experimental waveform for the anisotropic mudstone where two arrivals due to shear-wave birefringence, labelled S_{fast} and S_{slow}, can be seen. This waveform was detected using the point source thermal mechanism (radially polarized shear waves) and a PZT shear transducer for the Rx orientated parallel to the microlamination. The Rx was then rotated by 090° so as to be

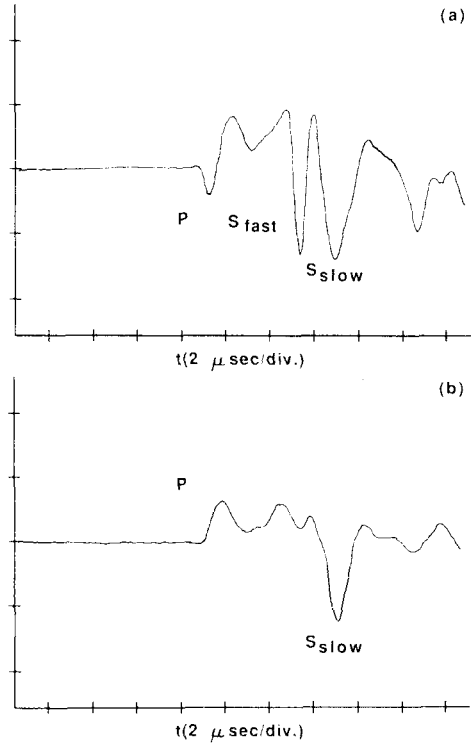

Figure 8. Waveforms for a circular thermoelastic laser source mechanism in anisotropic mudstone. (a) waveform for radially polarized laser source with PZT receiver polarized parallel to microlamination. (b) Waveform for radially polarized laser source with PZT receiver polarized perpendicular to microlamination.

perpendicular to the microlamination. The resulting waveform is shown in Fig. 8(b) and exhibits a dominant slow shear-wave arrival, but little evidence of a fast shear wave.

The velocities of the three wave modes were estimated from the waveforms of Fig. 8. The compressional wave velocity is 3800 ms^{-1}, with a fast shear-wave velocity of 2375 ms^{-1} and a slow shear-wave velocity of 2110 ms^{-1}. These values are within the range of those measured using a PZT source and give a value of 265 ms^{-1} for the shear-wave birefringence.

The measurements were then repeated with a cylindrical lens in the laser beam to produce a line source thermal expansion source mechanism. Fig. 1(a) indicates that the dipoles created by thermal expansion are perpendicular to the line orientation. The first experiment, therefore, had the Rx in the 090° direction parallel to the microlamination, with the laser line source at 000° such that the dipolar stresses were parallel to the Rx polarization direction. The resulting waveform is shown in Fig. 9(a) and contains both a fast and slow shear-wave arrival. The presence of a slow shear wave in this source receiver configuration (Fig. 8a and Fig. 9a) is thought to be caused by anisotropic thermal expansion of the source and is being investigated further. The laser source and PZT receiver were then rotated in parallel, so that both the dipolar forces in the laser line source and the polarization direction of the Rx were perpendicular to the microlamination. The waveform in this case (Fig. 9b) contained only a low-frequency slow-wave component.

The laser line source and PZT receiver were then repositioned such that the dipolar forces in the source were perpendicular to the receiver Rx. Fig. 9(c) is the recorded waveform when the Rx is parallel to the microlamination (090°), showing a predominant fast-shear mode.

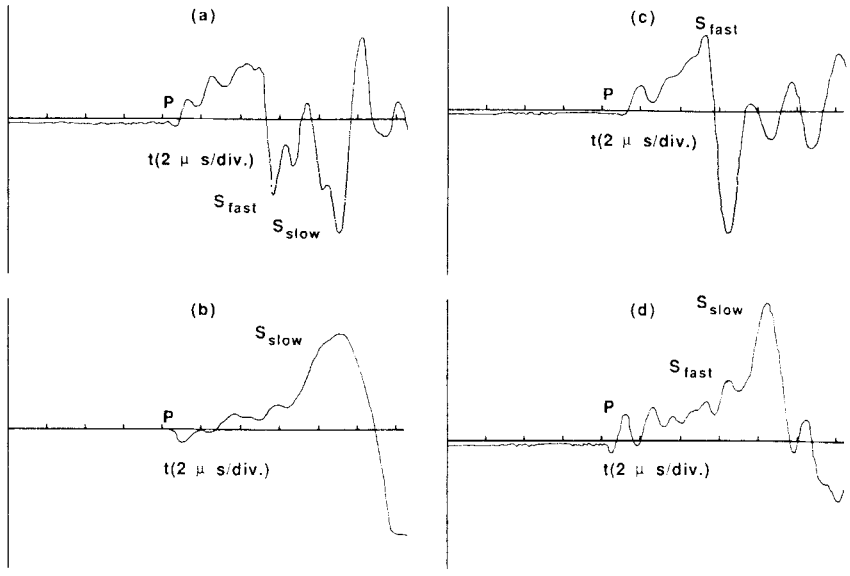

Figure 9. Waveform for a line thermoelastic laser source mechanism in anisotropic rock. (a) Waveform for laser and Rx polarizations parallel to microlamination. (b) Waveform for laser and Rx polarizations perpendicular to microlamination. (c) Waveform for laser polarization perpendicular and Rx polarization parallel to microlamination. (d) Waveform for laser polarization parallel and Rx polarization perpendicular to microlamination.

Fig. 9(d) shows the waveform for the same perpendicular source/receiver geometry but with the Rx perpendicular to the anisotropy (000°). In this case, the slow shear-wave mode is predominant.

Waveforms were also recorded using enhanced focusing and a thin layer of vacuum grease on the rock surface. This results in the source mechanism schematically represented in Fig. 2, which is dominated by preferential radiation of compressional waves in the epicentral position. Using a 5 MHz shear receiver, the waveform shown in Fig. 10 was recorded with Rx perpendicular to the microlamination. It should be observed that a prominent compressional wave signal and a slow shear-wave arrival are present.

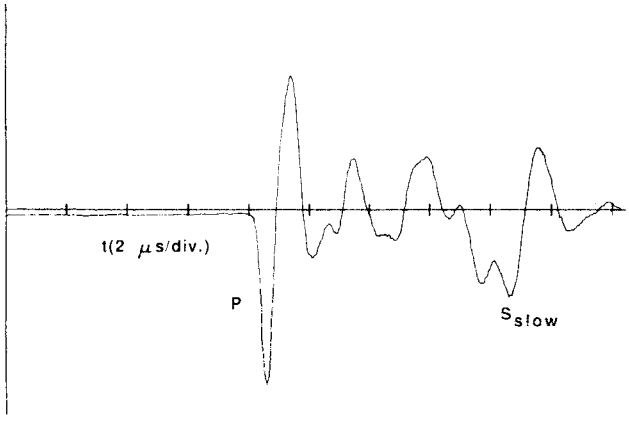

Figure 10. Waveform for an evaporation laser source mechanism in anisotropic mudstone: grease coated surface with circular focused laser source and Rx polarized perpendicular to microlamination.

4.3 DISCUSSION AND COMPARISON OF RESULTS

In the first set of measurements, a pair of matched PZT shear-wave transducers was rotated in a specially designed polariscope, for the study of propagation of selected shear-wave polarizations through isotropic halite and anisotropic calcite. It was demonstrated that the apparatus constructed could measure shear-wave birefringence in the latter sample ($450\,ms^{-1}$). Rotation of the shear-wave transducers allowed the fast (Fig. 5a) and slow (Fig. 5c) shear-wave components to be isolated and demonstrated there were unique directions along the crystal planes in which these components were polarized. These directions, as well as being analogous to optical birefringence, were in the same orientations as their optical counterparts. Shear-wave birefringence was also measured in the mudstone sample ($270\,ms^{-1}$), with the fast-shear mode travelling parallel to the microlamination and the slow mode perpendicular to the microlamination. It can also be seen from Figs 5(d) and 6(d) that the amplitude of the fast shear mode in the fast direction is larger than the amplitude of the slow mode in the slow direction. These diagrams confirm the predominance of two shear waves in the samples, with amplitudes being a maximum for the given modes parallel to their mode axes, regardless of the orientation of the Tx.

Measurements undertaken in mudstone using the laser source show good agreement with the above in that the birefringence value was similar ($265\,ms^{-1}$ for the mudstone sample studied). This shows that the technique has promise for measurements in rock samples. The waveform showed the expected trends when a comparison was made with theoretical waveforms of Figs 1 and 2, noting that the shear-wave transducers were velocity sensors. With a circular thermal expansion laser source mechanism, the waveform (Fig. 8a) recorded with Rx parallel to the anisotropy (090°) contained both fast and slow shear-wave arrivals, but only the slow wave was observed with Rx at 000°. The absence of a significant fast wave with Rx at 000° agrees with the former PZT measurements. The laser source generates all three wave modes (compressional and two shear) simultaneously and the waveform of Fig. 8(a) indicates that with Rx orientated appropriately, all three wave velocities can be estimated in a single measurement. This removes the requirement for rotation of shear-wave transducers, a major source of inaccuracy in PZT experiments. It should be noted that the circular source is symmetrical and hence rotation of the source would have no effect.

Waveforms recorded with a laser line source showed similar trends to the above. With the source stresses and Rx parallel to the anisotropy (Fig. 9a), all three wave modes were again observed, but only the slow shear wave was prominent with the two transducers rotated in unison by 90° (Fig. 9b). This laser-source mechanism has directional properties with stresses perpendicular to the line, so it was interesting to note the effect when the stresses were perpendicular to the Rx orientation. This was studied in Fig. 9(c) and (d) where it was evident that fast or slow shear waves could be selected by orientating Rx parallel or perpendicular to the anisotropy, respectively.

A final point to note is that evaporation of a coating led to a large compressional-wave signal (Fig. 10), despite the fact that a shear-wave transducer was used as a receiver. With a fixed Rx orientation, it is therefore possible to obtain clear signals for compressional (Fig. 10) and the two shear-wave components (Fig. 8a), with a single fixed piezoelectric shear-wave detector and two mechanisms of laser generation.

5 Conclusions

Pulsed laser generation of ultrasonic waves can be used to estimate the elastic parameters of rocks. The method offers certain advantages over traditional PZT techniques in that it is

non-contacting, the source parameters are controllable with the aid of additional lenses and the bandwidth is broader than most PZT transducers. The results for anisotropic mudstone showed that the technique could be used to determine the ultrasonic birefringence in the sample with a single, fixed PZT shear-wave transducer and two modes of laser source mechanism. The compressional and shear velocities obtained were comparable to those determined from traditional PZT (Tx–Rx) techniques.

In order to verify the laser technique, an ultrasonic polariscope was constructed to allow shear waves to be propagated at different orientations to the anisotropy in mineral and rock samples. The polariscope was calibrated using crystals of isotropic halite and anisotropic calcite. The results showed no birefringence for halite with strong ultrasonic birefringence for calcite, as would be expected. The polariscope allowed individual components of triaxial waveforms to be collected so that pseudo particle-motion diagrams could be constructed. The pseudo particle motion diagrams for the mudstone sample confirmed the expected particle motion for split shear waves and identified the orientation of anisotropy for Tx polarizations non-coincident with anisotropy.

The combination of a laser source and non-contacting laser interferometer as a receiver offers many opportunities for the remote sensing of rock physical properties in the laboratory. Scanning experiments in rocks for transducer directivity patterns and ultrasonic tomographic imaging are two of the applications such a system would promote. Preliminary experiments with this combination were not successful because of the loss of sensitivity in the interferometer over traditional PZT transducers. Focused orthogonal laser beams may also be one way to overcome the problem of measuring the three components of ultrasonic waveforms necessary for the construction of particle motion diagrams. These novel approaches are being developed at Queen's University for remotely studying the internal physical structure of low-loss materials and will be extended to rock and mineral specimens, as the sensitivity of the interferometer is improved.

Acknowledgments

The authors would like to thank the Natural Sciences and Engineering Research Council of Canada, Queen's University and Imperial Oil Limited (Canada) for their financial support. The authors are also grateful to John Evans, an undergraduate thesis student, for his help in collecting some of the PZT data.

References

Aleksandrov, K. S., 1956a. Special case of the propagation of elastic waves in crystals, *Soviet Physics – Crystallography*, **1**, 104–106.

Aleksandrov, K. S., 1956b. Propagation of elastic waves along specific directions in crystals, *Soviet Physics – Crystallography*, **1**, 563–570.

Bamford, D. & Crampin, S., 1977. Seismic anisotropy: the state of the art, *Geophys. J. R. astr. Soc.*, **49**, 1–8.

Bonner, B. P., 1974. Shear wave birefringence in dilating granites, *Geophys. Res. Lett.*, **1**, 217–220.

Byerly, P., 1938. The earthquake of July 6, 1934: amplitudes and first motions, *Bull. seism. Soc. Am.*, **24**, 81–99.

Christensen, N. I., 1971. Shear wave propagation in rocks, *Nature*, **229**, 549–550.

Christensen, N. I. & Ramananantoandro, P., 1971. Elastic moduli and anistropy of dunite to 10 kilobars, *J. geophys. Res.*, **76**, 4003–4010.

Crampin, S., 1985. Evaluation of anisotropy by shear wave splitting, *Geophysics*, **50**, 142–152.

Crampin, S., Chesnokov, E. M. & Hipkin, R. G., 1984. Seismic anisotropy – the state of the art: II, *Geophys. J. R. astr. Soc.*, **76**, 1–16.

Hudson, J., 1981. Wave speeds and attenuation of elastic waves in material containing cracks, *Geophys. J. R. astr. Soc.*, **64**, 113–150.

Hutchins, D. A., 1986. Mechanisms of pulsed photoacoustic generation, *Can. J. Phys.*, **64**, 1247–1263.

Hutchins, D. A. & Wilkins, D. E., 1985a. Elastic waveforms using laser generation and electromagnetic acoustic transducer detection, *J. appl. Phys.*, **58**, 2469-2477.

Hutchins, D. A. & Wilkins, D. E., 1985b. Polarized shear waves using laser line sources and electromagnetic acoustic transducer detection, *Appl. Phys. Lett.*, **47**, 789–791.

Hutchins, D. A., Young, R. P. & Ungar, J., 1985. Laser generated ultrasonic waves for the investigation of porous solids, *Proc. NATO Advanced Study Conference on Ultrasonic Methods in Evaluation of Inhomogeneous Materials, Tripani, Italy.*

Jolly, R. N., 1956. Investigations of shear waves, *Geophysics*, **21**, 905–938.

Musgrave, M. J. P., 1954a. On the propagation of elastic waves in aeolotropic media. I. General principles, *Proc. R. Soc. A*, **226**, 339–355.

Musgrave, M. J. P., 1954b. On the propagation of elastic waves in aeolotropic media. II. Media of hexagonal symmetry, *Proc. R. Soc. A*, **226**, 356–366.

Musgrave, M. J. P., 1970. *Crystal Acoustics*, Holden Day, San Francisco.

Nur, A. & Simmons, G., 1969a. Stress induced velocity anisotropy in rock: an experimental study, *J. geophys. Res.*, **74**, 6667–6674.

Nur, A. & Simmons, G., 1969b. the effect of saturation on velocity in low porosity rocks, *Earth planet. Sci. Lett.*, **7**, 183–193.

Pao, Y. H. & Gajewski, R. R., 1977. The generalized ray theory and transient responses of layered elastic solids, in *Physical Acoustics*, vol. 13, pp. 183–265, Academic Press, New York.

Tillman, S. E. & Bennett, H. F., 1973. Ultrasonic birefringence as a test of homogeneous elastic anisotropy, *J. geophys. Res.*, **78**, 7623–7629.

Vlaar, N. J., 1968. Ray theory for an anisotropic inhomogeneous elastic medium, *Bull. seism. Soc. Am.*, **58**, 2053–2072.